# 3D Dental Arch Curve Detection from CBCT Images and Its Applications to Tooth Segmentation

Benxiang Jiang[1,2[0000−0001−5135−7630]], Songze Zhang[1,2[0000−0003−4548−4363]], Jingyi Lyu[1,2[0009−0005−4822−8877]], and Hongjian Shi*[1,2[0000−0001−8732−4101]]

[1] Beijing Normal-Hong Kong Baptist University, Zhuhai, China
[2] Hong Kong Baptist University, Hong Kong, China
shihj@uic.edu.cn

**Abstract.** The three-dimensional (3D) dental arch curve, representing the spatial trajectory of dentition in either the maxilla or mandible, exhibits systematic alignment of tightly and orderly arranged teeth along its path. This structural configuration underscores its critical role as comprehensive anatomical guidance in digital dentistry, enabling high-precision tooth segmentation. In this study, we present a novel method for 3D dental arch curve detection from the volumetric cone beam computed tomography (CBCT) image, which, to our knowledge, represents the first successful implementation of 3D dental arch curve detection from the volumetric data. Specifically, we: (1) formulates and validates a dental arch curve fitting function, (2) identifies 3D uniformly distributed feature points proximal to the true dental arch curve through a feature point network framework, and (3) optimizes model parameters of the fitting function through a modified Expectation-Maximization (EM) algorithm with gradient descent. The proposed detection is then used to guide tooth segmentation through the curvilinear volume parameterization that unwind the vicinity of the dental arch curve. Experimental results demonstrate the accuracy for 3D dental arch curve detection and performance enhancements in the downstream task of tooth segmentation, improving segmentation precision compared to conventional approaches.

**Keywords:** CBCT · 3D Dental Arch Curve · Tooth Segmentation · EM Algorithm · Digital Dentistry.

## 1 Introduction

The dental arch constitutes the curved arrangement of teeth within the maxilla or mandible, with its morphology typically characterized through parametric curve representations [17, 5, 16]. Along this critical anatomical feature, teeth exhibit precise spatial organization and are systematically and tightly aligned. For volumetric data processing, this anatomical feature enables the extraction of dentition region-of-interest (ROI) since the dental arch curve's vicinity works as

a filter to preserve diagnostically relevant dentition regions as illustrated in Fig. 1.

The dental arch in the volumetric data set is three-dimensional (3D) that preserves authentic spatial inter-tooth relationships. However, current researches reveal an absence of robust algorithms for the detection of the 3D dental arch curve. Existing algorithms have succeeded in detecting dental arch curves with two-dimensional (2D) cone beam computed tomography (CBCT) projections [16, 29, 14] or three-dimensional (3D) dental mesh surfaces [22, 19, 30] through arch point detection and subsequent curve interpolation. In 3D volumetric space, on the other side, the critical challenge lies in reliably detecting arch points within the 3D CBCT image. This detection challenge hindering progress in detecting true 3D dental arch from the 3D CBCT image.

A specific curve can be described either by interpolation [11] or fitting [2] from given points. Interpolation defines the curve by passing through all given points and so require high accurate and reliable point detection. Fitting, on the other hand, utilizes given points to estimate parameters of a function. The function with estimated parameters fits a curve. In 3D dental arch curve detection from the volumetric data, detecting feature points uniformly distributed around the true 3D dental arch is practicable. Thus, fitting presents a more sensible strategy for 3D dental arch curve detection. Fitting based 3D dental arch curve detection involves three main challenges: 1. Formulation of a fitting function for the dental arch curve that suits the dental arch arrangement; 2. Automated detection of uniformly distributed feature points along the dental arch trajectory; and 3. Robust parameter estimation with latent variables that connect the feature points and the fitting function.

To resolve these challenges, this study proposes a three-stage fitting-based method for 3D dental arch curve detection in the 3D CBCT image as shown in Fig. 1. The method comprises: 1. A parametric curve equation to fit the dental arch curve; 2. A feature point network framework to identify uniformly distributed feature points proximal to the true dental arch curve; 3. A modified Expectation-Maximization (EM) algorithm [8] with the gradient descent [3] to optimize parameters and latent variables.

The clinical applications of 3D dental arch curves are primarily in guiding tooth segmentation, the task that segments and numbers individual tooth within the 3D CBCT image. Therefore, we also propose a curvilinear volume parameterization method based on the 3D dental arch curve in this study, as illustrated in Fig. 1. Through this parameterization, the dentition region within the CBCT image can be transformed into two curvilinear volumes as two narrow cuboid volumes specifically designed to localize the maxillary and mandibular dentitions, respectively. Within each curvilinear volume, all maxillary or mandibular teeth are closely and orderly arranged from left to right and constitute the dominant region of the space. In contrast, within the original CBCT image, teeth exhibit an arch-shaped arrangement, and the dentition occupies only a minor portion of the overall volume. Consequently, compared to performing segmentation directly within the CBCT space, our proposed curvilinear volume parameterization

method, based on the 3D dental arch curve, serves as an effective plug-and-play tool to enhance the accuracy of existing tooth segmentation methods. To validate the efficacy of the curvilinear volume parameterization method based on the 3D dental arch curve, we conducted comprehensive tests using several baseline segmentation methods, including nnUNet 2D [12], nnUNet 3D [13], SegResNet [21], and MedNext [23]. The experimental results demonstrate that curvilinear volume parameterization, functioning as a plug-and-play tool, effectively improves tooth segmentation accuracy.

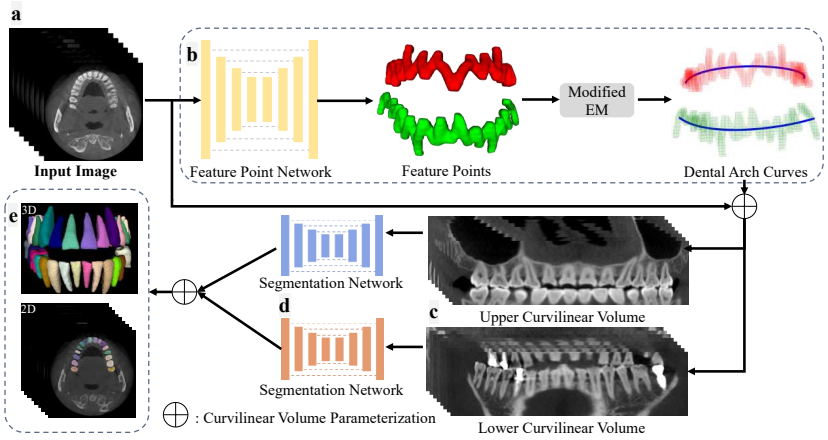


**Fig. 1.** Overview of the proposed method for fitting 3D dental arch curves, and serving as a plug-and-play tool for segmenting individual teeth from a 3D CBCT image. a. The input 3D CBCT image. b. Proposed 3D dental arch curve detection. c. Curvilinear volume parameterization to transform the CBCT image into two narrow cuboid volumes where teeth are closely and orderly arranged from left to right. d. Tooth segmentation implementation in the curvilinear volumes. e. Curvilinear volume parameterization to transform the segmented teeth into the CBCT image.

## 2 Methods

### 2.1 Dental Arch Curve Fitting Function

Contemporary orthodontic research emphasizes that any plan of dental arch determination must be flexible enough to produce arches varying in form through a parabola, cubic parabola, etc. [5]. Therefore, our 3D dental arch curve fitting function is a parametric curve that combines two cubic parabolas and a linear polynomial to capture both anatomical curvature and alveolar bone orientation:

$$\boldsymbol{C}(u) = (x(u), y(u), z(u)) = \begin{pmatrix} \theta_1 u + \theta_2 u^2 + \theta_3 u^3 + \theta_4 \\ \theta_5 u + \theta_6 u^2 + \theta_7 u^3 + \theta_8 \\ \theta_9 u^2 + \theta_{10} u + \theta_{11} \end{pmatrix} \tag{1}$$

where $u \in [0, 1]$ parameterizes the dental arch trajectory in the DICOM coordinate system (x-axis: Left to Right, y-axis: Anterior to Posterior, z-axis: Inferior

to Superior) [28] and $\{\theta_1, \ldots, \theta_1 1\}$are unobserved parameters for curve fitting. The parametric curve in Equation (1) achieves both anatomical fidelity and computational efficiency. The cubic parabola terms describe the natural variations and smooth transitions of the arch-shaped structure of the dental arch curve. The parabola term approximates the orientation of the alveolar bone. The 11 parameters in Equation (1) balances complexity of the fitting function and the optimization feasibility. The three polynomial expressions in Equation (1) enable derivatives for parameter estimation.

### 2.2 Feature Point Network Framework

Our feature point network framework processes a 3D CBCT image to uniformly distributed feature points along the maxillary and mandibular dental arch trajectories, as illustrated in Fig. 1. The critical component of the framework is ground truth generation. After collecting ground truths, we employ a 3D residual encoder U-Net [1, 13] implemented within the nnU-Net framework [12]. The nnU-Net framework automatically configures hyperparameters verified in segmentation tasks [13, 9]. This approach transforms the feature point detection task into a simpler binary volume segmentation problem. All segmented foreground voxels within the network output can subsequently be utilized as feature points for dental arch curve detection.

We propose an algorithm to generate ground truth feature points from manual tooth segmentation masks [7, 15], addressing the labor-intensive challenges of manual feature point annotation along 3D dental arches. The procedure initiates by fitting a parabolic curve to the axial projection of tooth centroids:

$$\xi(x) = \beta_1 x + \beta_2 x^2 + \beta_3 \tag{2}$$

where parameters $\beta_1, \beta_2, \beta_3$ are optimized through least squares estimation [27] from the axial coordinates of all maxillary/mandibular tooth voxels. To ensure uniform feature point distribution, the parabola in Equation (2) undergoes uniform discrete sampling by $x_n = t((n - 0.5)d),\ n \in \{1, ..., N\}$, where $t(\cdot)$ represents the inverse function of the arc length function of the parabola, $d$ is the interval, and $N$ specifies the feature point count. At each discrete point $x_n$, the orthogonal plane perpendicular to the tangent vector of $x_n$ is computed as $x + (\beta_1 + 2\beta_2 x_n)y - x_n - (\beta_1 + 2\beta_2 x_n)\xi(x_n) = 0$. Feature points are defined as centroids of the intersection areas between these planes and the maxillary/mandibular tooth volumes. These centroids are encoded in 3D label maps with label 1 for maxillary feature points and label 2 for mandibular feature points and processed with 555 morphological dilation to create network training targets. This automated pipeline ensures anatomical accuracy while eliminating manual annotation inconsistencies.

### 2.3 Modified EM algorithm with Gradient Descent

EM algorithm is an iterative statistical estimation method, particularly effective for parameter optimization in latent variables [8]. Its robustness in handling

latent variables makes it particularly suitable for 3D curve fitting challenges. The parameter estimation for Equation (1) employs a modified Expectation-Maximization (EM) framework that integrates gradient descent optimization [3] to address latent variable challenges in 3D curve fitting. This hybrid approach combines the statistical rigor of EM with numerical optimization capabilities.

The initialization step begins with ordered feature point coordinates $\{\boldsymbol{P}_1, \ldots, \boldsymbol{P}_N\} = \{(x_1, y_1, z_1), \ldots, (x_N, y_N, z_N)\}$ sorted by ascending $x$-values. Each feature point associates with a latent parameter $u_i$ for $i \in \{1, \ldots, N\}$, initialized through centripetal parameterization [4]: $u_i = u_{i-1} + \frac{\|\boldsymbol{P}_i - \boldsymbol{P}_{i-1}\|_2^{1/2}}{\sum_{j=2}^{N} \|\boldsymbol{P}_j - \boldsymbol{P}_{j-1}\|_2^{1/2}}$, with $u_1 = 0$. The error function quantifies cumulative deviation by $E = \sum_{i=1}^{N} \|\boldsymbol{P}_i - \boldsymbol{C}(u_i)\|_2^2$. In the maximization step, the partial derivative $\frac{\partial E}{\partial \theta_x} = 0$ gives the update for $\theta_x = (\theta_1, \theta_2, \theta_3, \theta_4)$, with analogous updates for $\theta_y = (\theta_5, \theta_6, \theta_7, \theta_8)$ and $\theta_z = (\theta_9, \theta_{10}, \theta_{11})$. In the Expectation step, the latent variables $u_1, \ldots, u_N$ are optimized via gradient descent with learning rate $\eta$: $u_i^{(k+1)} = u_i^{(k)} - \eta \frac{\partial E}{\partial u_i}$, $i = 1, \ldots, N$ where superscript $k$ denotes iteration index. $\frac{\partial E}{\partial u_1}, \ldots, \frac{\partial E}{\partial u_N}$ are computed through chain rule differentiation of the error function. In the iteration step, iteration alternates between coefficient updates and latent variable optimization until convergence or fixed iteration numbers. This dual optimization strategy combines the global convergence properties of EM with local refinement through gradient descent, thus balancing efficiency and accuracy.

### 2.4 Curvilinear Volume Parameterization

Given a fitted dental arch curve $\boldsymbol{C}_{fit}(u)$, we define tubular coordinates as $\{(x, y, z) | (x, y, z) = \boldsymbol{C}_{fit}(u) + \alpha \boldsymbol{B}(u) + \gamma \boldsymbol{N}(u), u \in [0, 1], \alpha \in [-40, 40], \gamma \in [t_1, t_2]\}$, where $\boldsymbol{T}(u) = \frac{\boldsymbol{C}'_{fit}(u)}{|\boldsymbol{C}'_{fit}(u)|}$, $\boldsymbol{N}(u) = \frac{\boldsymbol{T}'(u)}{|\boldsymbol{T}'(u)|}$, and $\boldsymbol{B}(u) = \boldsymbol{T} \times \boldsymbol{N}$ are the unit tangent, normal, and binormal vectors, $[t_1, t_2] = [-40, 56]$ for the maxillary teeth and $[-56, 40]$ for the mandibular teeth. Let the length of $\boldsymbol{C}_{fit}(u)$ with $u \in [0, 1]$ be $L$. This tubular coordinates unwinds the vicinity of the dental arch curve $\boldsymbol{C}_{fit}(u)$ into a rectilinear 3D volume $V \in \mathcal{R}^{L \times 80 \times 96}$ through discretely sampling $R_v$ at $\Delta u = 1/L$, $\Delta\alpha = \Delta\gamma = 1$ using bicubic interpolation and $(u, \alpha, \gamma) \leftarrow (x, y, z)$ via diffeomorphic mapping. This unwinding process is reversible naturally.

## 3 Experiments and Discussions

### 3.1 Materials

This study utilizes a hybrid dataset of 110 3D CBCT images with corresponding voxel-level tooth segmentation ground truth volumes, comprising 98 cases from [7, 6] and 12 cases from [15]. The dataset [7, 6] contains 4531 CBCT volumes, of which 148 are publicly available. Among these 148 volumes, 50 are small field-of-view (FOV) CBCT images lacking complete maxillary and mandibular structures, while the remaining 98 large FOV CBCT volumes constitute our utilized subset. The dataset [15] comprises 12 CBCT volumes, all of which were

employed in this study. The hybrid dataset encompasses 15 distinct acquisition protocols with spatial resolutions ranging from $0.25\times0.25\times0.27$ mm$^3$ to $0.4\times0.4\times0.4$ mm$^3$ and field-of-view dimensions spanning $12.1\times12.1\times8.51$ cm$^3$ to $16\times16\times13.1$ cm$^3$. To address the absence of manual tooth numbering, we implemented the FDI World Dental Federation notation system [10] as illustrated in Fig. 1 through manual labeling, creating a classification strategy comprising 33 distinct anatomical categories: 32 permanent tooth identifiers (combining 4 jaw quadrants and 8 tooth types) plus background.

### 3.2 Experimental Setup

Experiments were performed on a GIGABYTE G292-Z42 workstation featuring an Intel Xeon Platinum 8352V processor, NVIDIA RTX 4090 GPU, NVIDIA L20 GPU, and 64GB DDR4 memory, operating under Ubuntu 22.04 LTS. From the complete dataset of 110 CBCT scans with voxel-level annotations, we employed stratified sampling to construct training (88 cases) and testing (22 cases) cohorts while preserving anatomical diversity and scanner manufacturer balance. The training set comprised 79 scans from [7, 6] and 9 cases from [15], while the test set included 19 scans from [7, 6] and 3 from [15]. This partitioning strategy ensured representative coverage of both conventional and challenging dental arch morphologies across different imaging protocols.

### 3.3 Feature Point Detection Performance

Since the detected feature points reside within the CBCT volumetric space and are represented as small cubic regions, feature point detection accuracy was quantified through the Dice Similarity Coefficient (DSC) [25], defined as $DSC = \frac{2|P\cap G|}{|P|+|G|}$, where $P$ and $G$ denote predicted and ground truth feature point regions. The range of DSC is [0,1], with a larger value indicating better prediction accuracy. As shown in Fig. 2(a), our feature point network achieves mean DSC scores of $85.39 \pm 3.81\%$ (maxillary feature points, Class 1) and $83.9 \pm 0.036\%$ (mandibular feature points, Class 2), demonstrating its localization accuracy. Notably, case 5 (DSC= 74.43% for Class 1) and case 9 (DSC= 72.39% for Class 2) presented unique challenges: case 5 exhibited metal artifacts in the maxillary region with partial dentition loss, while case 9 contained two impacted mandibular wisdom teeth with associated positional anomalies.

Visual analysis of these challenging cases as shown in Figs. 2(b)-(c) revealed three main characteristics: True positive regions (blue regions) consistently captured essential dental arch trajectory features despite anatomical complexities; false negative regions (red regions) predominantly occurred in interproximal regions where feature point ambiguity naturally exists; and false positive regions (green regions) localized to regions excluded from natural dental arch trajectory, specifically metal artifacts in case 5 and impacted mandibular wisdom teeth in case 9. This strategic error distribution patterns in Figs. 2(b)-(c) indicate the feature point network learned to prioritize anatomically meaningful feature points.

### 3.4 Dental Arch Curve Fitting Analysis

The convergence characteristics of our modified EM algorithm are demonstrated through progressive curve fitting outcomes across multiple iterations as shown in Fig. 2(d). Employing 1,000 gradient descent steps with a conservative learning rate $\eta = 1 \times 10^{-6}$ per EM iteration, the method achieves acceptable accuracy within just one iteration cycle. While increased iterations (10-50) further refine the fit, diminishing returns become evident, as evidenced by near-identical 10- and 50-iteration fitting function curves in Fig. 2(d). This rapid convergence stems from the algorithm's hybrid optimization strategy that synergizes partial derivative parameter solutions with gradient descent-based latent variable updates. Computational efficiency analysis reveals linear time scaling relative to iteration count, with single-iteration processing requiring $0.394 \pm 0.047$ seconds for maxilla and $0.367 \pm 0.052$ seconds for mandible seconds and 10 iterations requiring $3.664 \pm 0.414$ seconds for maxilla and $3.643 \pm 0.549$ seconds for mandible. The network's ability to maintain feature points' anatomical plausibility, even in suboptimal detection scenarios, confirms its robustness for the subsequent dental arch curve fitting procedure.

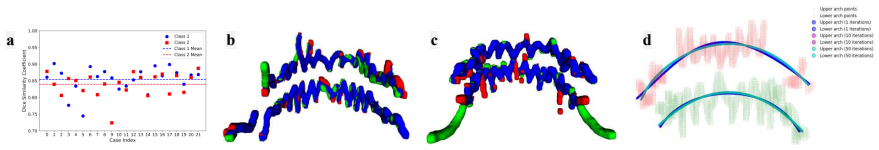


**Fig. 2.** Evaluations of dental arch curve detection. a. Accuracy of feature point detection. b. Feature point detection results of Case 5. c. Feature point detection results of case 9. d. A case for dental arch curve fitting with 1, 10, and 50 EM iteration cycles.

### 3.5 Feasibility Analysis of Dental Arch Curve Fitting Function

When defining the fitting function in Equation (1), we assume that this fitting function can fit a 3D dental arch curve that primarily lies around a plane. This hypothesis of dental arch morphology was validated through geometric analysis of 220 fitted curves (110 in maxilla, 110 in mandible) from their corresponding ground truth feature points. For each fitted curve, we computed the optimal approximation plane by minimizing the orthogonal distance. All orthogonal distances are larger than 0, with mean orthogonal deviation of $0.053 \pm 0.056$ mm. This confirms the feasibility of our parametric curve fitting function in capturing the near-planar 3D dental arch curve.

### 3.6 Curvilinear volume parameterization for tooth segmentation

We propose curvilinear volume parameterization to establish 3D dental arch detection as a plug-and-play tool for tooth segmentation.To validate this tool's efficacy, we compared four popular segmentation architectures: nnU-Net 2D [12],

nnU-Net 3D [13], SegResNet [21], and MedNext [23]. For each architecture, training and testing were performed separately on both: (1) the original 3D CBCT volumes, and (2) their transformed cuboid volumes generated through curvilinear volume parameterization. Comparative analysis extends to recent tooth segmentation methods [6, 14, 18, 26, 24, 20] with their reported performance metrics and 3D CBCT images used. Quantitative results are presented in Table 1. Let TP, TN, FP, FN represent true positives, true negatives, false positives, and false negatives, three metrics [25] quantify segmentation accuracy including $Dice = \frac{2TP}{2TP+FP+FN}$, $Precision = \frac{TP}{TP+FP}$, and $Recall = \frac{TP}{TP+FN}$. Experimental results show that the dental arch curve successfully guides tooth segmentation, achieving segmentation metrics equivalent to state-of-the-art methods.

**Table 1.** Comparison with existing methodologies in individual tooth segmentation

| Methodology | Dental arch guide | 3D CBCT images used | Metrics (%) | | |
|---|---|---|---|---|---|
| | | | Precision | Dice | Recall |
| nnUNet 2D [12] | No | 110 | 74.05 | 72.15 | 71.34 |
| | Yes | | 93.83 | 93.57 | 93.30 |
| nnUNet 3D [13] | No | 110 | 74.07 | 72.37 | 72.77 |
| | Yes | | 93.72 | 93.91 | 94.09 |
| SegResNet [21] | No | 110 | 74.47 | 73.34 | 74.25 |
| | Yes | | 93.66 | 93.88 | 94.10 |
| MedNext [23] | No | 110 | 74.10 | 72.66 | 73.34 |
| | Yes | | 94.33 | 94.33 | 94.32 |
| Cui et al. [6] | - | 20 | - | 91.98 | - |
| Jang et al. [14] | - | 97 | 95.97 | 94.79 | 93.71 |
| Li et al. [18] | - | 350 | 92.13 | 91.13 | 91.23 |
| Tan et al. [26] | - | 314 | - | 95.78 | - |
| Shaheen et al. [24] | - | 186 | - | 90 | - |
| Liu et al. [20] | - | 451 | - | 94.3 | - |

## 4 Acknowledgments

This work was supported in part by the Guangdong Higher Education Key Platform and Research Project under Grant 2020ZDZX3039, in part by the Guangdong Provincial Key Laboratory of Interdisciplinary Research and Application for Data Science under Grant 2022B1212010006.

## 5 Conclusion

This study first proposes 3D dental arch curve detection from volumetric CBCT image and demonstrates that precise 3D dental arch curve detection serves as a plug-and-play tool for automated tooth segmentation. Experimental results show our 3D dental arch curve detection is accurate and robust. The dental arch curve guided tooth segmentation benchmarking methodologies are much more accurate than the corresponding benchmarking methodologies without dental arch curve guide.

## References


1. Alom, M.Z., Yakopcic, C., Hasan, M., Taha, T.M., Asari, V.K.: Recurrent residual u-net for medical image segmentation. Journal of medical imaging **6**(1), 014006–014006 (2019)
2. Alpaydin, E.: Machine learning. MIT press (2021)
3. Andrychowicz, M., Denil, M., Gomez, S., Hoffman, M.W., Pfau, D., Schaul, T., Shillingford, B., De Freitas, N.: Learning to learn by gradient descent by gradient descent. Advances in neural information processing systems **29** (2016)
4. Balta, C., Öztürk, S., Kuncan, M., Kandilli, I.: Dynamic centripetal parameterization method for b-spline curve interpolation. IEEE Access **8**, 589–598 (2019)
5. Braun, S., Hnat, W.P., Fender, D.E., Legan, H.L.: The form of the human dental arch. The Angle Orthodontist **68**(1), 29–36 (1998)
6. Cui, W., Wang, Y., Zhang, Q., Zhou, H., Song, D., Zuo, X., Jia, G., Zeng, L.: Ctooth: a fully annotated 3d dataset and benchmark for tooth volume segmentation on cone beam computed tomography images. In: International Conference on Intelligent Robotics and Applications. pp. 191–200. Springer (2022)
7. Cui, Z., Fang, Y., Mei, L., Zhang, B., Yu, B., Liu, J., Jiang, C., Sun, Y., Ma, L., Huang, J., et al.: A fully automatic ai system for tooth and alveolar bone segmentation from cone-beam ct images. Nature communications **13**(1), 2096 (2022)
8. Do, C.B., Batzoglou, S.: What is the expectation maximization algorithm? Nature biotechnology **26**(8), 897–899 (2008)
9. Duan, Y., Wang, P., Huang, Y., Hang, Y., Sun, Q., Shao, H., Yang, J.: Optimizing semi-supervised medical image segmentation with imbalanced filtering and nnu-net enhancement. The Visual Computer pp. 1–13 (2025)
10. Federation, F.W.D.: The 2018 fdi policy statements. International Dental Journal **69**(1), 3 (2020)
11. Hagan, P.S., West, G.: Interpolation methods for curve construction. Applied Mathematical Finance **13**(2), 89–129 (2006)
12. Isensee, F., Jaeger, P.F., Kohl, S.A., Petersen, J., Maier-Hein, K.H.: nnu-net: a self-configuring method for deep learning-based biomedical image segmentation. Nature methods **18**(2), 203–211 (2021)
13. Isensee, F., Wald, T., Ulrich, C., Baumgartner, M., Roy, S., Maier-Hein, K., Jaeger, P.F.: nnu-net revisited: A call for rigorous validation in 3d medical image segmentation. In: International Conference on Medical Image Computing and Computer-Assisted Intervention. pp. 488–498. Springer (2024)
14. Jang, T.J., Kim, K.C., Cho, H.C., Seo, J.K.: A fully automated method for 3d individual tooth identification and segmentation in dental cbct. IEEE transactions on pattern analysis and machine intelligence **44**(10), 6562–6568 (2021)
15. Jiang, B., Zhang, S., Shi, M., Liu, H.L., Shi, H.: Alternate level set evolutions with controlled switch for tooth segmentation. IEEE Access **10**, 76563–76572 (2022)
16. Kwon, T., Choi, D.i., Hwang, J., Lee, T., Lee, I., Cho, S.: Panoramic dental tomosynthesis imaging by use of cbct projection data. Scientific reports **13**(1), 8817 (2023)
17. Lee, S.J., Lee, S., Lim, J., Park, H.J., Wheeler, T.T.: Method to classify dental arch forms. American journal of orthodontics and dentofacial orthopedics **140**(1), 87–96 (2011)
18. Li, P., Liu, Y., Cui, Z., Yang, F., Zhao, Y., Lian, C., Gao, C.: Semantic graph attention with explicit anatomical association modeling for tooth segmentation from cbct images. IEEE Transactions on Medical Imaging **41**(11), 3116–3127 (2022)

19. Lin, G., Yang, S., Chen, Y., Xu, Q., Yap, P.T., Yun, Z., Feng, Q.: Transfarchnet: Predicting dental arch curves based on facial point clouds in personalized panoramic x-ray imaging. Expert Systems with Applications p. 126577 (2025)
20. Liu, Y., Xie, R., Wang, L., Liu, H., Liu, C., Zhao, Y., Bai, S., Liu, W.: Fully automatic ai segmentation of oral surgery-related tissues based on cone beam computed tomography images. International Journal of Oral Science **16**(1), 34 (2024)
21. Myronenko, A.: 3d mri brain tumor segmentation using autoencoder regularization. In: International MICCAI brainlesion workshop. pp. 311–320. Springer (2018)
22. Qiu, L., Ye, C., Chen, P., Liu, Y., Han, X., Cui, S.: Darch: Dental arch prior-assisted 3d tooth instance segmentation with weak annotations. In: Proceedings of the IEEE/CVF Conference on Computer Vision and Pattern Recognition. pp. 20752–20761 (2022)
23. Roy, S., Koehler, G., Ulrich, C., Baumgartner, M., Petersen, J., Isensee, F., Jaeger, P.F., Maier-Hein, K.H.: Mednext: transformer-driven scaling of convnets for medical image segmentation. In: International Conference on Medical Image Computing and Computer-Assisted Intervention. pp. 405–415. Springer (2023)
24. Shaheen, E., Leite, A., Alqahtani, K.A., Smolders, A., Van Gerven, A., Willems, H., Jacobs, R.: A novel deep learning system for multi-class tooth segmentation and classification on cone beam computed tomography. a validation study. Journal of Dentistry **115**, 103865 (2021)
25. Taha, A.A., Hanbury, A.: Metrics for evaluating 3d medical image segmentation: analysis, selection, and tool. BMC medical imaging **15**, 1–28 (2015)
26. Tan, M., Cui, Z., Zhong, T., Fang, Y., Zhang, Y., Shen, D.: A progressive framework for tooth and substructure segmentation from cone-beam ct images. Computers in Biology and Medicine **169**, 107839 (2024)
27. Theodoridis, S., Koutroumbas, C.: Pattern recognition: Elsevier inc (2009)
28. Treichel, T., Gessat, M., Prietzel, T., Burgert, O.: Dicom for implantations—overview and application. Journal of digital imaging **25**, 352–358 (2012)
29. Yun, Z., Yang, S., Huang, E., Zhao, L., Yang, W., Feng, Q.: Automatic reconstruction method for high-contrast panoramic image from dental cone-beam ct data. Computer methods and programs in biomedicine **175**, 205–214 (2019)
30. Zhong, X., Zhang, Z.: 3d dental biometrics: Automatic pose-invariant dental arch extraction and matching. In: 2020 25th International Conference on Pattern Recognition (ICPR). pp. 6524–6530. IEEE (2021)